

Journal: Landslides

Reference: LASL-D-17-00172 R2

Paper title: New, simplified and improved interpretation of the Vaiont landslide mechanics

Authors: Alan P. Dykes ^{1*}, Edward N. Bromhead ²

Author affiliations: ¹ Centre for Engineering, Environment and Society Research, School of Engineering, Kingston University, Penrhyn Road, Kingston upon Thames, KT1 2EE, U.K.
a.p.dykes@kingston.ac.uk
² 9 Kevins Drive, Yateley, Hampshire, GU46 7TL, U.K.

Correspondence: * Corresponding author (A P Dykes). Address and Email shown above.
Tel.: +44 (0)208 417 7018

Abstract: Both the occurrence *and* behaviour of the Vaiont landslide have not been satisfactorily explained previously because of difficulties arising from the assumption that the failure surface was ‘chair’ shaped. It is now known that there was no ‘chair’, which means that the 1963 landslide could not have been a reactivated ancient landslide because the residual strength of the clay interbeds would have been insufficient for stability prior to 1963. Furthermore, the moderately translational geometry reduces the influence of reservoir-induced groundwater and hence of submergence.

Standard stability analyses now show that prior to 1960, the average shear strength must have significantly exceeded the peak shear strength of the clay interbeds known to have formed the majority of the failure surface. Three-dimensional stability analyses confirm these results and show that at the time of the first significant movements in 1960, the rising reservoir level had a negligible effect on the Factor of Safety.

According to these results, the Vaiont landslide was most likely initiated by pore water pressures associated with transient rainfall-induced ‘perched’ groundwater above the clay layers, in combination with a smaller than hitherto assumed effect of reservoir impounding, then developed by brittle crack propagation within the clay beds, thus displaying progressive failure. Further very heavy rainfall accelerated the process, possibly due to reservoir-induced groundwater impeding drainage of the rainwater, until the limestone beds at the northeast margin failed. With the shear strength suddenly reduced to residual throughout, the entire mass was released and was able to accelerate as observed.

Key words: Vaiont, landslide, geotechnics, limit equilibrium, stability analysis, reservoir effects

New, simplified and improved interpretation of the Vaiont landslide mechanics

Alan P. Dykes ^{1*} and Edward N. Bromhead ²

¹ *Centre for Engineering, Environment and Society Research, School of Engineering, Kingston University, Penrhyn Road, Kingston upon Thames, Surrey, UK*

² *9 Kevins Drive, Yateley, Hampshire, UK*

*Corresponding author

Abstract

Both the occurrence *and* behaviour of the Vaiont landslide have not been satisfactorily explained previously because of difficulties arising from the assumption that the failure surface was ‘chair’ shaped. It is now known that there was no ‘chair’, which means that the 1963 landslide could not have been a reactivated ancient landslide because the residual strength of the clay interbeds would have been insufficient for stability prior to 1963. Furthermore, the moderately translational geometry reduces the influence of reservoir-induced groundwater and hence of submergence.

Standard stability analyses now show that prior to 1960, the average shear strength must have significantly exceeded the peak shear strength of the clay interbeds known to have formed the majority of the failure surface. Three-dimensional stability analyses confirm these results and show that at the time of the first significant movements in 1960, the rising reservoir level had a negligible effect on the Factor of Safety.

According to these results, the Vaiont landslide was most likely initiated by pore water pressures associated with transient rainfall-induced ‘perched’ groundwater above the clay layers, in combination with a smaller than hitherto assumed effect of reservoir impounding, then developed by brittle crack propagation within the clay beds, thus displaying progressive failure. Further very heavy rainfall accelerated the process, possibly due to reservoir-induced groundwater impeding drainage of the rainwater, until the limestone beds at the northeast margin failed. With the shear strength suddenly reduced to residual throughout, the entire mass was released and was able to accelerate as observed.

Key words Vaiont, landslide, geotechnics, limit equilibrium, stability analysis, reservoir effects

1 Introduction

The Vaiont landslide of 9 October 1963 was the most deadly and devastating landslide ever recorded in Europe, causing around 2000 fatalities, mostly due to the destruction of the town of

Longarone in the Piave valley, northern Italy (Fig. 1). The occurrence of the disaster, and the events leading up to it, are well-documented (Semenza 2001, 2010). Many attempts have been made to explain the occurrence and behaviour of the landslide, particularly the attainment by the moving mass of such a high velocity (usually reported as around 25-30 m s⁻¹: e.g. Müller 1964; Romero and Molina 1974; Hendron and Patton 1985; Kilburn and Petley 2003; Crosta et al. 2016). There has not yet been a single explanation that can satisfactorily account for all of the known evidence. A commemorative conference was held on the 50th Anniversary of the event, in order to review and re-examine some of the remaining technical questions (Genevois and Prestininzi 2013). Some results presented in the conference pre-empted part of our work but our interpretations are new and, we believe, significantly reposition the importance of the Vaiont landslide for future hazard and risk assessments of proposed dam projects in high mountain regions.

In a separate paper, we identified a scientific consensus regarding the Vaiont landslide that appeared to be almost universally accepted at the 50th Anniversary conference and beyond. This consensus comprises four elements that are listed in Table 1. However, following the presentation at the conference and subsequent publication of a newly-derived map of the geometry of the failure (Bistacchi et al. 2013) that corresponded with our own developing hypothesis regarding the landslide, we sought to examine the implications of this with regard to the previous evidence and interpretations published since 1963. Our review of the relevant evidence, including detailed examination of the extensive collection of photographs taken by Eduardo Semenza and colleagues in the years prior to 1963 (Masé et al. 2004) and of the various interpretations of seismic (Caloi 1966), hydrogeological and geotechnical (Müller 1964, 1968) monitoring data (e.g. Semenza 2001, 2010 and references therein) revealed critical early (mis)interpretations and oversights that allowed the consensus to develop and consolidate (Dykes and Bromhead – in press). We also proposed a new explanation for the geomorphological context of the landslide that can account for all of the known evidence.

The underlying premise of this paper is that the failure surface of the Vaiont landslide does not have a ‘chair’ shape (Dykes and Bromhead – in press). The logical consequences of this are that the 1963 landslide could not have been a reactivation of an ancient landslide. Without a ‘chair’, back-analysis of the stability of the slope yields peak, not residual, shear strength parameters. The residual strength of the clay seams would have been insufficient to hold the mass in place prior to 1963. Furthermore, the absence of a subhorizontal basal part of the failure surface significantly reduces the influence of reservoir-induced raised pore water pressures. This leads to a new hypothesis for the Vaiont landslide comprising four distinct but integrated elements that largely



Figure 1. Location of Longarone and the Vaiont landslide north of Venice (Venezia) in northern Italy. From Dykes and Bromhead (in press).

Table 1. Elements of the established consensus and the new hypothesis relating to the Vaiont landslide, showing reference codes used in this paper (from Dykes and Bromhead – in press).

Ref.	Element of the consensus	Ref.	Element of the new hypothesis
C1	The failure was a reactivation of an ancient landslide.	H1	The 1963 landslide was a first-time failure.
C2	Both the prehistoric landslide and the 1963 landslide took place along thin clay seams in a limestone mass and that these were at, or near, residual strength prior to 1960.	H2	Failure took place along thin clay seams in a limestone mass that were initially at peak strength.
C3	The shape of the sliding surface followed a folded rock structure that comprised a subhorizontal lower part and a steeply inclined upper part, commonly referred to in the literature as a 'chair' shape.	H3	The sliding surface did not have a 'chair' shape but was moderately translational.
C4	The trigger for the failure was a major loss in stability due to inundation of the toe of the slide mass by the impounded reservoir.	H4	The slope was geologically predisposed to fail but rainfall was the main preparatory factor. Inundation of the toe was the eventual trigger but this was probably insufficient on its own, only being effective in concert with heavy rainfall.

reject the consensus view (Table 1). In this paper we will apply routine geotechnical theory to the Vaiont landslide as defined geometrically by Bistacchi et al. (2013) to test this hypothesis and, in doing so, to provide an explanation for the landslide that can account for its occurrence *and* behaviour and is consistent with all of the evidence that we have been able to access.

2 Geology and the failure surface

2.1 Geology

The stratigraphy of the Vaiont landslide, which comprises a sequence of Jurassic-Cretaceous limestones of varying lithologies, is summarised in Table 2. [Hendron and Patton \(1985\)](#) confirmed both the presence and stratigraphic continuity of clay interbeds within the Fonzaso and Calcare di Socchèr Formations, particularly upwards from the basal failure surface within the Fonzaso Formation. Failure occurred along many of the major clay layers in different parts of the slope but [Hendron and Patton \(1985, p.18\)](#) noted that ‘...at least one layer of clay occurred several metres above the surface of sliding of the 1963 slide. This clay layer was thicker than any found at the base of the 1963 slide.’ The possibility of (perched) aquicludes within the landslide mass must therefore be acknowledged.

The variable character of the internal geological structures of the mountain slope and the landslide mass arises from a tectonic history that produced, among other local features, complex interference patterns between the southern limb of the eastward-plunging Erto Syncline and the steeply plunging Massalezza Syncline ([Massironi et al. 2013](#)). The apparent ‘roughness’ of the exposed failure surface reflects the accommodation of the tectonic compression within the bedding sequence as well as some post-1963 modifications due to stress relief, weathering and rockfalls ([Massironi et al. 2013](#); [Wolter et al. 2014](#)). However, a further consequence is that some parts of the stratigraphy became locally densely fractured, promoting preferential groundwater flow as well as severely limiting the recovery of intact cores from boreholes drilled in 1960 ([Hendron and Patton 1985](#)).

The critical conclusions from Massironi et al.’s study, consistent with our own views, are that the tectonic movements and deformations, across as well as along bedding, probably controlled and

Table 2. Indicative stratigraphy of the south side of the Vaiont valley (after [Bistacchi et al. 2013](#) and [Ghirotti et al. 2013](#)).

Age	Stratigraphy	Thickness
Paleocene	Scaglia Rossa	~300 m
Upper Cretaceous		
Cretaceous	Calcare di Socchèr (or ‘Biancone Formation’)	150 m
Upper Jurassic	Rosso Ammonitico	0–15 m
	Fonzaso Formation	10–40 m
Middle Jurassic	Vajont Limestone	350–450 m

even promoted formation of the failure surface along different clay-rich beds within the stratigraphy, and that the highly variable patterns of tectonic fracturing throughout the in situ rocks also predisposed the northern slope of Mt Toc to potential instability. The development of the 1963 landslide and the form of its failure surface can therefore be fully attributed to the inherent geology (lithology and stratigraphy) and tectonic history of the site and it can be described as a ‘bedding-controlled rockslide’ or indeed a very large ‘dip-slope failure’.

2.2 Shape of the concealed failure surface

The Vaiont landslide is perhaps best known for its ‘chair’ shaped failure surface in 2D cross-section, which has confounded investigations into its occurrence for more than half a century (e.g. [Romero and Molina 1974](#); [Hendron and Patton 1985](#); [Nonveiller 1992](#); [Pinyol and Alonso 2010](#); [Paronuzzi and Bolla 2012](#)). The ‘chair’ structure is associated with the eastward-dipping southern limb of the Erto syncline. However, it was deformed by NE-SW tectonic compression which formed the Massalezza syncline ([Massironi et al. 2013](#)) and created a bowl-shaped 3D structure. [Bistacchi et al. \(2013\)](#) presented a new 3D digital model of the failure surface shape (Fig. 3) that confirmed our own early hypothesis and partially verified some of the earliest post-failure accounts ([Kiersch 1964](#); [Müller 1964, 1968](#); [Broili 1967](#)). The key elements are the general eastward dip of up to 20° of the bedding within around 500 m of the gorge, and the consequent steep and most likely stepped failure zone cutting through many of the stratigraphically higher limestone beds near the eastern margin (although the ‘steps’ would hardly be visible on scaled cross-sections). The latter provided a deep zone of high resistance to movement (e.g. east of Bistacchi et al.’s profile ‘E’: Fig. 3), particularly in the lower eastern side, that restricted movements here and gave rise to the observed movement patterns elsewhere ([Müller 1964](#)).

3 Methodology

3.1 General approach

Analysis of the stability of a slope that has already failed, so-called ‘back analysis’, is a routine method for many landslide investigations that is often used to estimate mean mobilised values for the shear strength of the failed slope at the instant of failure. This approach to problems in geotechnical engineering has a long pedigree and can be used with total stresses ([Skempton 1948](#)) and effective stresses (e.g. [Hutchinson 1969](#); [Chandler 1977](#)) although the latter is preferred. Such static analyses require information on the pre-failure geometry of the topographic surface, sliding

surface and any other relevant internal geological structures, the geotechnical properties of the materials involved including density and shear strength, and the distribution and magnitude of water pressures in the slope.

Most of the previously published quantitative analyses of the stability of Mt Toc have been ‘standard’ back analyses using limit equilibrium approaches, although some researchers have utilised kinematic simulations to investigate the landslide (e.g. [Alonso and Pinyol 2010](#); [Havaej et al. 2015](#)). We use limit equilibrium back analyses as the framework for our arguments because, as explained below, more sophisticated methods are not needed to explain the Vaiont landslide given that there is no ‘chair’. Strictly, 3-dimensional analyses are necessary to accommodate the bowl-shaped failure surface that was indicated soon after the landslide occurred although many studies have utilised more routine 2D analyses. The latter are sufficient for us to demonstrate the critical arguments but we then use 3D results to verify our conclusions. We have used the Morgenstern-Price method of analysis in 2D and a variant of Hungr’s method in 3D ([Bromhead 2004](#); [Hungr 1987, 1989](#)).

3.2 Geotechnical considerations

Limit equilibrium stability analyses calculate the ratios of ‘driving forces’ (‘D’) to ‘resisting forces’ (‘R’) in order to obtain a Factor of Safety, with the occurrence of movement resulting from the net force, i.e. $D - R$. The landslide mass will accelerate if $D > R$ and will decelerate when $D < R$. If it is not moving, $R \geq D$. In a rotational landslide, D will start to reduce immediately as the landslide starts to move due to changing moments about the centre of rotation, whereas in a translational landslide there is no such reduction due to geometric change. At Vaiont, $D > R$ must have been maintained without significant reduction for at least 15 seconds in order to account for the movement rate, at a shear strength half of that before the onset of movement. This would suggest a dominantly translational rather than rotational geometry, i.e. that there was no ‘chair’ structure.

Developing this argument further, we can use the ‘chair’ geometry (i.e. a compound landslide comprising rotational and translational components) to discount several previously long-held interpretations of the Vaiont landslide. If the landslide mass is represented as two blocks as shown in Fig. 2A, a back-analysis gives a shear strength of $\phi' = 8-12^\circ$ and $c' = 0$, where ϕ' is the effective angle of internal friction and c' is the effective cohesion. Such a value can only correspond with the residual strength of a clay, which would suggest that the 1963 landslide involved reactivation of a much older pre-existing landslide. Without a ‘chair’, the back-analysed shear strength is much higher.

If the landslide moves (Fig. 2B), Block 1 (i.e. all mass downslope of the vertical hinge line) becomes larger and Block 2 becomes smaller, which reduces D as in a rotational slide. The reservoir level rises, which increases external resistance. Therefore the net force $D - R$ starts to reduce almost immediately. Block 2 must also get round the ‘corner’ (i.e. past the ‘hinge’ of the ‘chair’ shape), which requires (i) a large-scale pre-existing internal rupture (raising further questions about how the original landslide may have occurred) or (ii) substantial internal shearing which will take energy out of the system due to the higher resulting R (e.g. [Romero and Molina 1974](#)).

If the shear strength was initially at residual, the landslide mass would have been approximately in equilibrium with the disturbing gravitational force and the observed acceleration would not have been possible. Furthermore, there is now duplicate evidence of retrogression of the heads of both sides of the 1963 landslide scar (see Section 5.4). With reference to Fig. 2C, if the top part of Block 2 is not included, there is insufficient mass on the slope to overcome a even residual friction angle as low as $\phi' = 9^\circ$. In other words, if the landslide is ‘chair-shaped’, the top part of the mass is essential if there is to be enough thrust to overcome the resistance at the bottom (Block 1 plus external water).

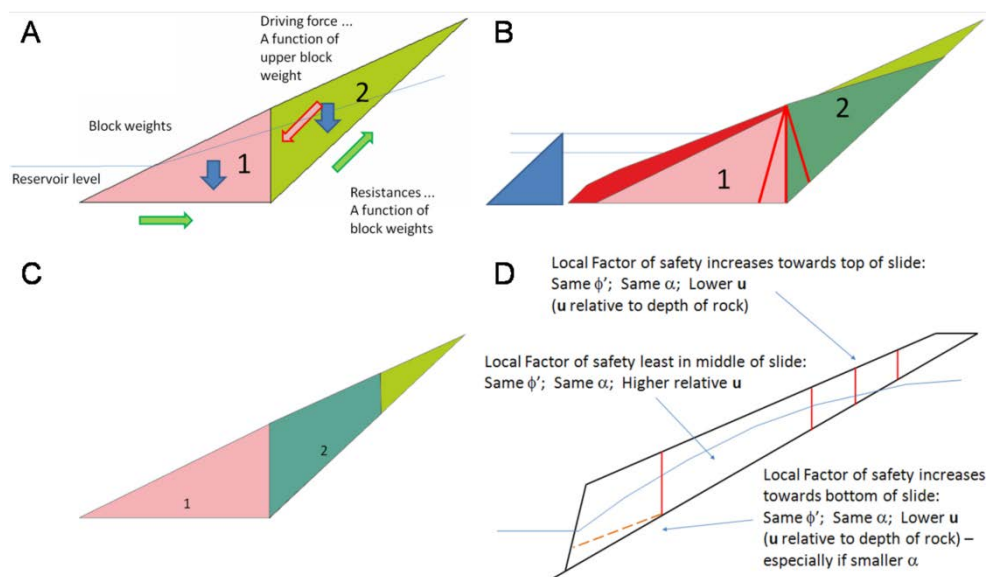


Figure 2. Slope stability principles that negate the ‘chair’ hypothesis. (A) Simple representation of the problem with a ‘chair’ structure. (B) Internal and external changes affecting a hypothetical ‘chair’-shaped landslide. (C) Loss of driving force if the upper part of Block 2 is not included. (D) Simple representation of how the local Factor of Safety varies along a translational landslide.

If the landslide has a translational geometry and the relative pore pressure distribution of Fig. 2D, the local Factor of Safety is lowest in the middle part and the bottom must move with the middle if it fails, but the top may be left behind due to the local Factor of Safety increasing upslope. This is because pore water pressures would normally be higher in the lower parts of the slope due to downslope seepage contributing to a higher (or even perched) water table (Fig. 2D).

Therefore, if the 1963 landslide was a first-time failure, the higher ϕ' implied by the back-analysis must have represented the peak strength. Consequently, the shear strength reduction of the clay layers from peak to residual is sufficient to produce the conditions required to account for the rapid acceleration and large displacement of the unstable mass. Thus, if there is no (or very little) 'chair', the whole of the 1963 failure cannot have been an ancient landslide because the mass could not have remained in place until 1963 at residual strength. The consensus position therefore cannot account for the occurrence, acceleration or retrogressive development of the landslide.

Finally, the consensus position also cannot fully account for the observed patterns of movement of the landslide. Rates of ground movement correlated strongly with rainfall irrespective of reservoir level (Müller 1964; Hendron and Patton 1985) but there is no evidence of artesian groundwater below the clay layers that gave rise to the failure surface (Dykes and Bromhead – in press). Indeed, it now appears that the landslide was underdrained and probably largely devoid of significant water pressures except following periods of very heavy rainfall when transient perched water tables may have formed above the clay layers. This is the only reasonable explanation for the observed correlation of measured movement rates with rainfall throughout 1960-63. Limited data from three piezometers (Müller 1964; Hendron and Patton 1985; Dykes and Bromhead – in press) show that the limestones above and below the clay layers responded to rainfall and to external reservoir water very quickly. Unfortunately, there are no data that can provide any evidence for the perched water tables within the landslide mass or for the impacts of reservoir impoundment on them, but reference base-line conditions can be reasonably assumed (Section 3.3).

3.3 Pore pressure assumptions

The pore water pressures acting on the failure surface at the time of failure are unknown, although they were most likely hydrostatic pressures below a transient perched water table contained entirely within the landslide mass. Because the landslide appears to have been underdrained and may therefore have been mostly devoid of significant water pressures for much of the time (Dykes and

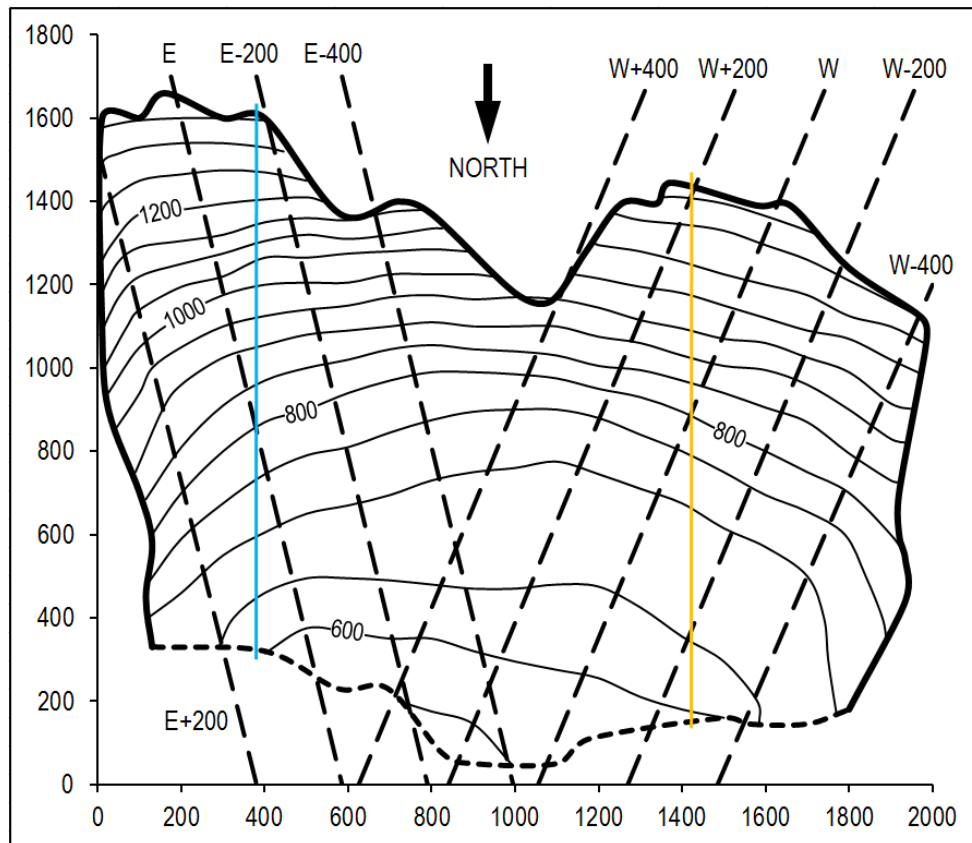


Figure 3. Failure surface map with x - y axes in metres and contours at 50 m intervals, showing lines of cross-sections analysed in this paper. The light blue line is E (N-S) and the orange line is W (N-S). Failure surface contours and Sections ‘E’ and ‘W’ after [Bistacchi et al. \(2013\)](#).

[Bromhead – in press](#)), we started by back-analysing a completely dry slope. In any case, this produces a minimum possible value for the required minimum friction angle along the slip surface on which we base our conclusions. It is inconceivable that there were no pore pressures within the landslide at the time of failure. Indeed, we must infer that there were possibly significant raised pore pressures for short periods of time following heavy rainfall. If such transient water pressure conditions did arise, then the effective stresses would have been correspondingly lower, so that the computed angle of shearing resistance must be higher than calculated with the zero pore water pressure assumption. The shear stress is unaffected by the pore pressure assumptions in the analysis as it is a function only of geometry and unit weight. The shear stress is unaffected by the pore pressure assumptions in the analysis as it is a function only of geometry and unit weight.

Analysis of the effects of part submergence seems, regrettably, to be poorly understood, notwithstanding the publication by [Bishop \(1955\)](#) of a method of dealing with it. Matters are not helped by the publication of completely wrong theories (e.g. [de Mello et al. 2002](#)). In essence, there

are two competing effects: (i) external loading on the lower part of the landslide surface, an effect that always improves stability and therefore reduces the required shear strength for equilibrium calculated in a back analysis; (ii) the introduction or modification of water pressures in the slope (Bromhead et al. 1999), which always reduces stability and therefore increases the calculated shear strength needed for equilibrium. It is therefore not possible to make a back analysis where the slope is submerged *and* this is believed to be a factor in its instability – and yet to neglect the (unknown) pore pressure effect. A problem therefore arises: what was the initial pore pressure state prior to submergence, and what effect does submergence have on the pore pressure distribution? This is a case where the result obtained is entirely dependent on the assumptions made. Moreover, the effect of pore water pressure on shear strength is somewhat dependent on the density of the soil or rock involved as the higher the density, the smaller the effect of pore pressure, and vice versa.

At Vaiont, if the piezometric line was higher than external reservoir level before the toe of the landslide was submerged, then the calculation always yields an improvement in stability because the reservoir provided external support with no change to the internal conditions. Conversely, the maximum negative effect from submergence would have arisen from internal pore water pressures increasing from zero to values associated with a horizontal piezometric line at the level of the external water surface. Our analysis assumes the latter case, which has a smaller effect in practice and may be similar to actual conditions prior to the final failure. However, the critical point is that the pore water pressure effect is significantly greater for an assumed ‘chair’ shape than it is for the moderately translational failure surface established by Bistacchi et al. (2013). We do not consider the effects of possible transient perched water tables affecting part of the failure surface above the horizontal piezometric level. This is not a limitation because to do so would merely reinforce key parts of our arguments: we only need to show the minimum friction angles needed for stability in order to substantiate our case.

3.4 Input data

In the case of the Vaiont landslide, the pre-failure topography is known in detail from the maps of Rossi and Semenza (1965) and the failure surface geometry has been redefined by Bistacchi et al. (2013). For both the west and east sides of the landslide, Bistacchi et al. (2013) presented a representative longest cross-section aligned with the corresponding theoretical direction of movement (identified as ‘E’ and ‘W’). We have analysed these and parallel sections at 200 m intervals laterally (Figs. 3, 4). There are no other constraining geological structures, the failure being mostly defined by bedding structures approximately parallel to the failure surface. We have

also checked that these slope-parallel alignments were not influencing results by also analysing North-South profiles centred on the intersections of profiles W and E with the 800 m contour (also indicated in Fig. 4), with a further overall check being provided by the 3D analyses.

The assumed density of the rocks used in previous studies varies (Table 3), and there is some uncertainty about the most representative value. Limestone matrix is dominated by calcite (specific gravity $G = 2.71$; $\gamma = 26.6 \text{ kN m}^{-3}$) but the matrix density of a dolostone is slightly higher ($G = 2.87$; $\gamma = 28.2 \text{ kN m}^{-3}$) (Doveton 1999). Clay layers at 18 kN m^{-3} will reduce the overall rock mass unit weight by less than 0.5 kN m^{-3} (corresponding with 10% total volume of clay). The densely fractured nature of the rocks at Vaiont will necessarily reduce the actual density by a further very small fraction. Thus the landslide mass could have a unit weight of up to 26 kN m^{-3} in theory, even with a very small overall porosity, but the densely fractured mass and small volume occupied by clay must reduce this value, and the range of typical densities is almost always lower (Table 4). The value of rock density/unit weight used in analyses with no water in the slopes makes no difference to calculated shear strengths represented as friction angles. However, if there is water in the slopes, then the higher the density of the rock mass, the smaller are the relative effects of pre-existing pore water pressures and both internal and external effects from submergence of the slope. We have therefore analysed the 2D profiles using $\gamma = 20, 23$ and 26 kN m^{-3} to cover the range of possibilities.

3.5 Stability analyses

Firstly, we back-analysed 2D slope profiles using three unit weights ($\gamma = 20, 23$ and 26 kN m^{-3}):

1. For each unit weight, we determined the peak shear strength mobilised along each profile (Fig. 4) at the point of failure at $FS = 1.0$, represented as an (effective) angle of internal friction, ϕ_p' , for (a) no water and (b) water table elevation = reservoir level at 600 m, 650 m, 700 m and 722.5 m. The 650 m level corresponds with the end of the 'first filling' in November 1960, and 722.5 m was the design top water level for the reservoir.
2. For each unit weight, we determined the FS of each profile (Fig. 3) assuming $\phi_p' = 30^\circ$ throughout, for (a) no water and (b) water table elevation = reservoir level = 600 m, 650 m, 700 m and 722.5 m. The assumed value of ϕ_p' has no bearing on these results: the actual mobilised friction angle for each case, ϕ_m' , was not dependent on the assumed ϕ_p' .
3. For each unit weight, we determined the maximum reduction in FS of each profile (Fig. 4), assuming $\phi_p' = 30^\circ$ throughout, from 'no water' to water table elevation = reservoir level = 722.5 m.
4. We examined the possible effect of the 1960 landslide on the FS of 2D profiles W and W-200 by repeating step 2 (above) for these profiles with the thickness of the 1960 landslide removed.

Table 3. Published densities and unit weights assumed to apply to the Vaiont landslide at the time of failure.

Unit Weight (kN m ⁻³)	Reference
26 (relative density = 2.65)	Martinis (1978)
26.5 (relative density = 2.7)	Anderson (1985)
23.5	Alonso and Pinyol (2010)
26.3 – 26.5	Superchi (2012)
24.5	Del Ventisette et al. (2015)

Table 4. Derived unit weights of some Mesozoic limestones and dolostones (n.s. = not stated).

Limestone Formation	Dry – Saturated Unit Weight (kN m ⁻³)	Reference
Triassic		
Thaynes Limestone, Wyoming, USA	26.0 – 26.1	Manger (1963)
Ross Fork Limestone, Wyoming, USA	24.7 – 25.4	
Muschelkalk, Mutzig, Germany	26.3 – 26.4	
Muschelkalk, Galicia, Poland	24.1 – 25.4	
Limestone (part dolomitic), Switzerland	26.2 – 26.5	
Marble, Switzerland	25.9 – 26.2	
Jurassic		
Twin Creek Limestone, Wyoming, USA	27.0 – 27.0	Manger (1963)
Carmel formation (limestone), Utah, USA	26.0 – 26.2	
Solenhofen Limestone, Germany	25.2 – 25.6	
Limestone, Switzerland	25.8 – 26.1 25.2 – 25.8	
Inferior oolite, England	22.9 – 24.1	
Oolite, England	22.1 – 23.6	
White Lias, England	23.9 – 24.8	
Oolitic Jurassic limestone, England (various different named quarried beds)	20.7-23.6 – not stated	NCS (2017)
Oolitic Bioclastic limestone, England	18.0 – n.s. 19.6 – n.s.	
Middle Jurassic Oolitic Limestone from the Bath Oolite Horizon, England	19.5 – n.s. 20.9 – n.s.	
Portland limestone, England	24.9 – 25.8	
Portland Base Bed limestone, England	21.0 – n.s.	BRE (1997)
Cretaceous		
Caddo limestone, Texas, USA	25.3 – 25.7	Manger (1963)
Glen Rose Limestone, Texas, USA	21.7 – 23.2	
Peterson Limestone, Wyoming, USA	24.0 – 24.9	
Limestone, Switzerland	25.5 – 26.0	
MEAN:	23.5 – 25.6	

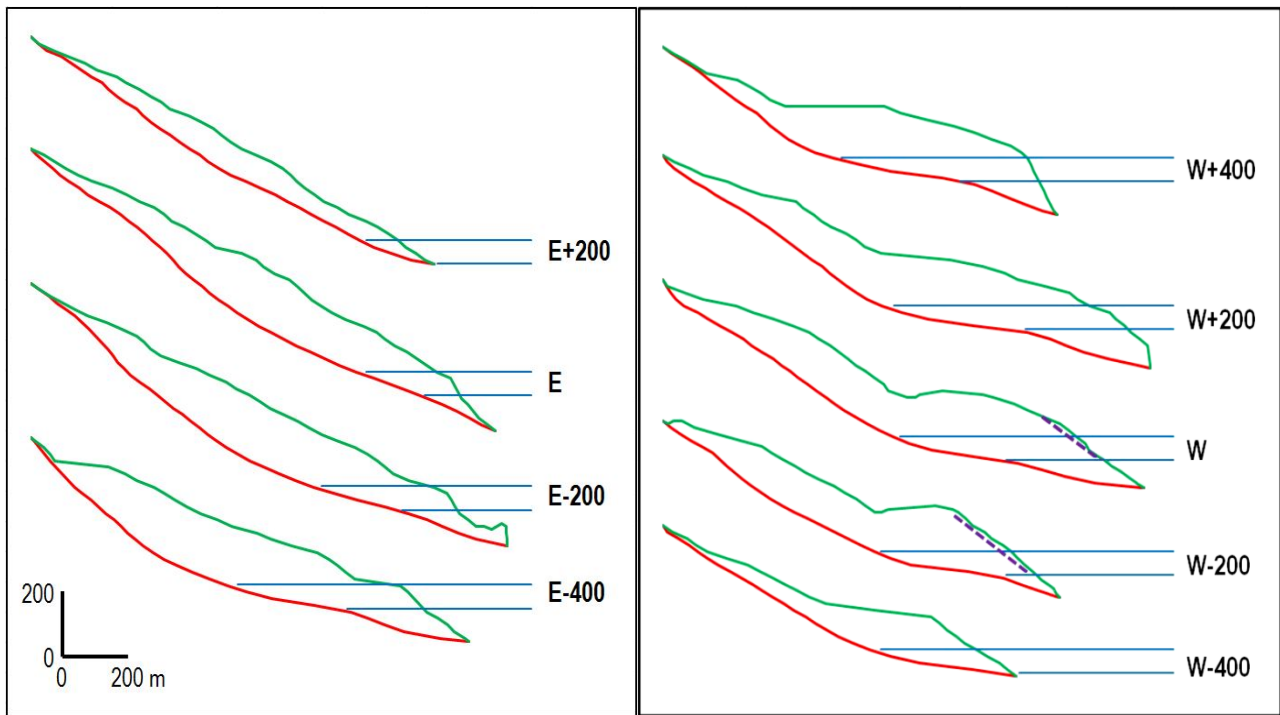


Figure 4. Analysed 2D slope profiles through the Vaiont landslide (Fig. 3). Reservoir and groundwater elevations of 650 m and 722.5 m are shown for each profile. The approximate position of the 1960 landslide (dashed line) is indicated on profiles W and W-200.

Secondly, we performed 3D stability analyses. Using the same source documents as for the cross-sections, the failure surface and the pre-failure topography were specified as elevations at the intersections of an arbitrarily-positioned 100 m \times 100 m x - y grid (as shown in Fig. 3), with the outline of the failed mass specified to the nearest 25 m. We analysed the landslide to assess the degree of variation of 2D results from the whole landslide condition, using $\gamma = 23 \text{ kN m}^{-3}$, $\phi_p' = 25^\circ$ and no cohesion, for (a) a completely dry slope and (b) water table elevation = reservoir level at 600 m, 650 m, 700 m and 722.5 m. Finally, the actual ϕ_m' for each case was calculated and confirmed as being independent of the assumed value for ϕ_p' , the latter having no bearing on these results.

4 Results

4.1 Results – mobilised friction angle

Results obtained from the 2D analyses are shown in Table 5 and Figs. 5-7. Table 5 shows the complete set of stress, friction angle and stability values obtained for each profile for $\gamma = 23 \text{ kN m}^{-3}$, including north-south versions of profiles E and W. All of these results (except for the N-S profiles)

were also obtained for $\gamma = 20$ and 26 kN m^{-3} . Figs. 5 and 6 illustrate the effects of the unit weight, which can be seen to be negligible in terms of the mobilized friction angle and very small in terms of Factor of Safety (FS) reductions due to water tables resulting from toe inundation. For the dry condition, the minimum angle of internal friction, ϕ' , required for stability along each section is significantly higher towards the eastern margin (Table 5; Fig. 5), and the western side of the landslide was more sensitive to changing water levels than the eastern side (Figs. 6, 7). This is consistent with the recorded observations of ground movements during 1960-63 that showed movement rates to be highest in the lower part of the west side, lower in the upper west side, much lower still in the upper east side and minimal in the lower east side (Müller 1964). The friction angles required for stability are lowest at profiles W+400 and W-400 (Fig. 5) because there is very little mass on the steeper upper part of the failure surface. The landslide of November 1960 would have reduced the FS of profiles W and W-200 by no more than 0.9% and 0.6% respectively (maximum changes for completely dry slopes), i.e. increasing the friction angle required for stability by around 0.1° . This represents at most a marginal effect for each of these 2D profiles, so the effect on the overall stability of the entire mountain slope must be considered negligible and need not be considered further.

The mean mobilised friction angle obtained from the analysed profiles is $\phi'_p = 22.0^\circ$ for a completely dry slope and $\phi'_p = 22.8^\circ$ with the water level at 722.5 m (c.f. Fig. 5). The peak friction angle (ϕ'_p) of clays such as those found within the Fonzaso Formation, no more than a few mm thick and interbedded with the limestones, probably fall within the range $\phi'_p = 22\text{--}26^\circ$ found in clays under normal stresses of 1–10 MPa, i.e. corresponding with the Vaiont case (Petley 1999, cited in Kilburn and Petley 2003). The higher friction angle required to maintain stability of the eastern side was provided by the weak clay beds being buried to ever increasing depths eastwards by the overlying younger limestones and by the available strength across and through the bedding of these younger rocks.

All of the 3D stability analyses showed the vector direction for the minimum FS to be almost exactly due North. The first 3D stability analysis of the entire landslide ($\gamma = 23 \text{ kN m}^{-3}$, $\phi'_p = 25^\circ$) gave FS = 1.03 (effective normal stress = 1969 kPa, shear stress = 895 kPa). For stability at FS = 1.0, the mobilized friction angle $\phi' = 24.4^\circ$, higher than the indicative mean value obtained from the separate 2D profile analyses but this must have been even higher to resist the adverse effects of even the lowest reasonable groundwater level and/or artesian pore water pressures (Hendron and Patton 1985). Reduction of the friction angle to 12° reduces the stability by half (FS = 0.5) and allows the observed acceleration when the last intact limestone beds failed on 9 October 1963.

Table 5. Results of 2D stability analyses of cross-sections through the Vaiont landslide (Figs. 4, 5) for a various slope conditions with unit weight = 23 kN m⁻³. Profiles E (N-S) and W (N-S) are the north-south versions of E and W.

Profile:	W (N-S)	W-400	W-200	W ¹	W+200	W+400	E-400	E-200	E ¹	E+200	E (N-S)
	Normal effective stress (kPa):										
Dry slope	2294	1457	2281	2501	2596	2376	2560	2160	1910	1095	2001
Reservoir at 600 m	2292	²	2277	2475	2541	2353	2519	²	1902	²	2001
Reservoir at 650 m	2267	²	2246	2401	2457	2294	2449	2083	1880	²	1987
Reservoir at 700 m	2159	1374	2139	2267	2301	2154	2322	2008	1830	1073	1947
Reservoir at 722.5 m	2092	1316	2072	2193	2217	2063	2248	1961	1800	1057	1918
Reservoir at 725 m	2084	1309	2064	2185	2207	2053	2240	1956	1796	1055	1915
	Shear stress (kPa):										
Dry slope	865	479	845	910	898	727	975	1025	1041	598	1042
Reservoir at 600 m	864	²	844	906	884	719	968	²	1037	²	1042
Reservoir at 650 m	854	²	832	891	860	697	949	1000	1027	²	1036
Reservoir at 700 m	836	468	811	864	825	660	918	976	1007	593	1023
Reservoir at 722.5 m	825	458	798	848	807	638	900	963	996	587	1014
Reservoir at 725 m	823	456	796	846	805	636	898	961	995	586	1013
	Angle of internal friction, ϕ' , for FS = 1.0:										
Dry slope	20.7°	18.2°	20.3°	20.0°	19.1°	17.0°	20.9°	25.4°	28.6°	28.7°	27.5°
Reservoir at 600 m	20.7°	²	20.3°	20.1°	19.2°	17.0°	21.0°	²	28.6°	²	27.5°
Reservoir at 650 m	20.6°	²	20.3°	20.4°	19.3°	16.9°	21.2°	25.6°	28.7°	²	27.5°
Reservoir at 700 m	21.2°	18.8°	20.8°	20.9°	19.7°	17.0°	21.6°	26.0°	28.8°	28.9°	27.7°
Reservoir at 722.5 m	21.5°	19.2°	21.1°	21.1°	20.0°	17.2°	21.8°	26.2°	29.0°	29.0°	27.9°
Reservoir at 725 m	21.6°	19.2°	21.1°	21.2°	20.0°	17.2°	21.8°	26.2°	29.0°	29.1°	27.9°
	Factor of Safety using $\phi' = 30^\circ$ throughout:										
Dry slope	1.53	1.75	1.56	1.59	1.67	1.89	1.52	1.22	1.06	1.06	1.11
Reservoir at 600 m	1.53	²	1.56	1.58	1.66	1.89	1.50	²	1.06	²	1.11
Reservoir at 650 m	1.53	²	1.56	1.56	1.65	1.90	1.49	1.20	1.06	²	1.11
Reservoir at 700 m	1.49	1.70	1.52	1.52	1.61	1.89	1.46	1.19	1.05	1.05	1.10
Reservoir at 722.5 m	1.46	1.66	1.50	1.49	1.59	1.87	1.44	1.18	1.04	1.04	1.09
Reservoir at 725 m	1.46	1.66	1.50	1.49	1.58	1.86	1.44	1.17	1.04	1.04	1.09

Notes

¹ Profile presented by [Bistacchi et al. \(2013\)](#)

² Failure surface always above this level or (at E-200 m) with negligible inundated mass at this level

4.2 Results – effective stresses

The data recorded during 1960-63 showed that from the start of the second filling of the reservoir in October 1961, the piezometric surfaces in three piezometers P1, P2 and P3 ([Müller 1964](#); [Hendron and Patton 1985](#)) rose gradually to meet the reservoir water level after periods of time related to each piezometer's distance upslope – and up-dip – from the Vaiont gorge ([Dykes and Bromhead – in press](#)). Thereafter, until the landslide occurred, they matched the changing external reservoir level almost exactly. The combined effect of the internal pore water pressures and the external

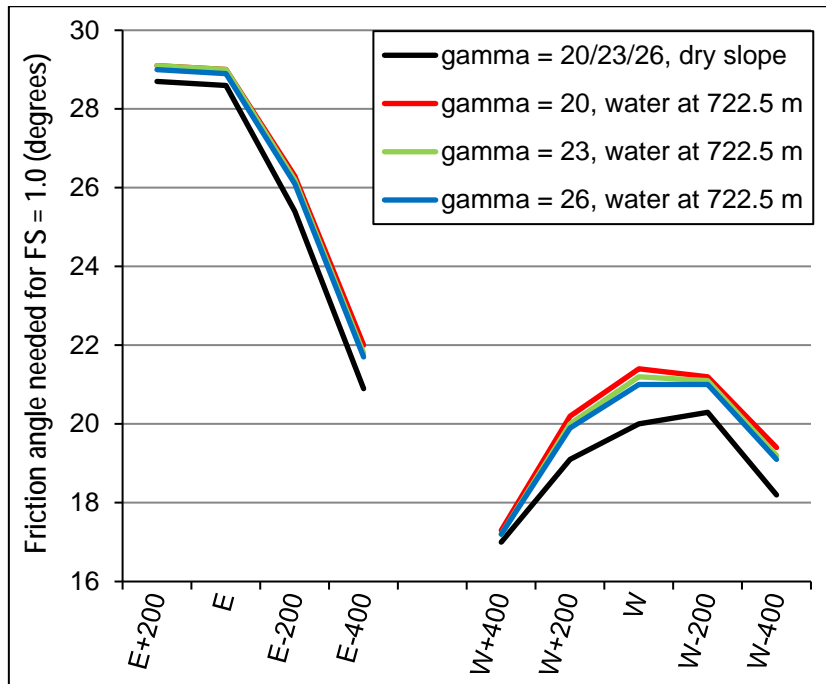


Figure 5. Mobilised friction angle ($c' = 0$) to maintain stability of each 2D profile for different unit weight assumptions ($\gamma = \gamma$, kN m^{-3}) under completely dry and maximum inundation water table conditions.

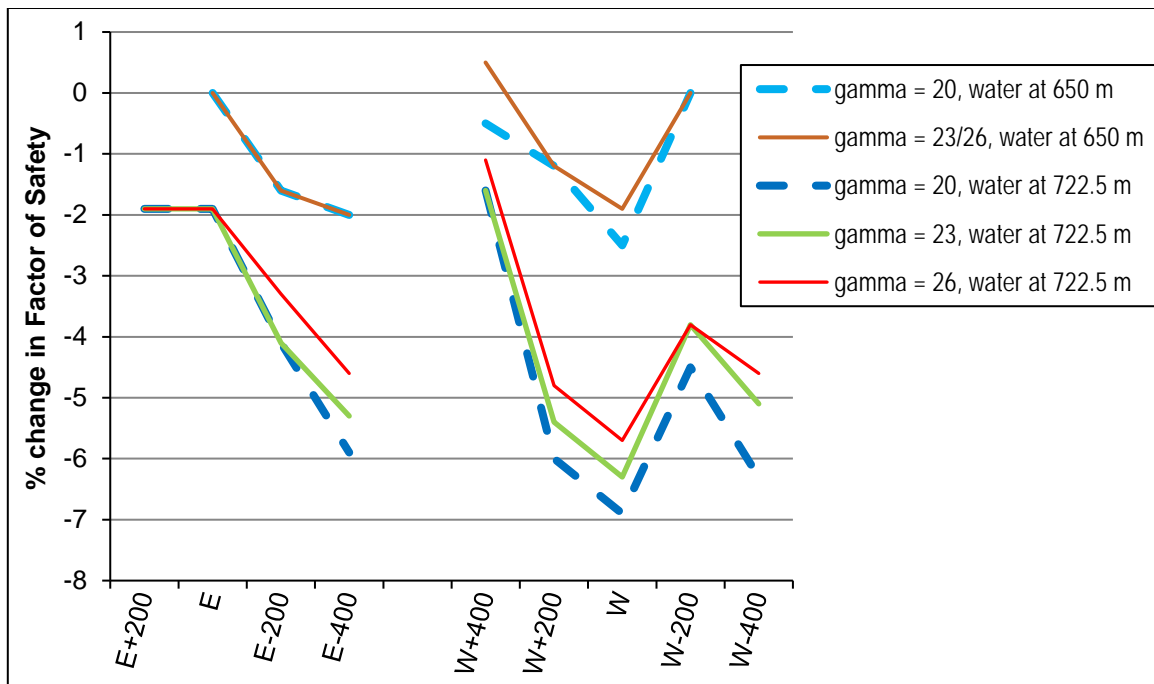


Figure 6. Reductions in the Factor of Safety from the dry slope condition at each 2D profile arising from different unit weight assumptions ($\gamma = \gamma$, kN m^{-3}) for 'first filling' (i.e. 650 m) and maximum inundation (i.e. 722.5 m) water table elevations. The lines for $\gamma = 23/26 \text{ kN m}^{-3}$ at water level = 650 m were identical throughout (like all lines for water = 650 m in the East side) so are shown as a single line here.

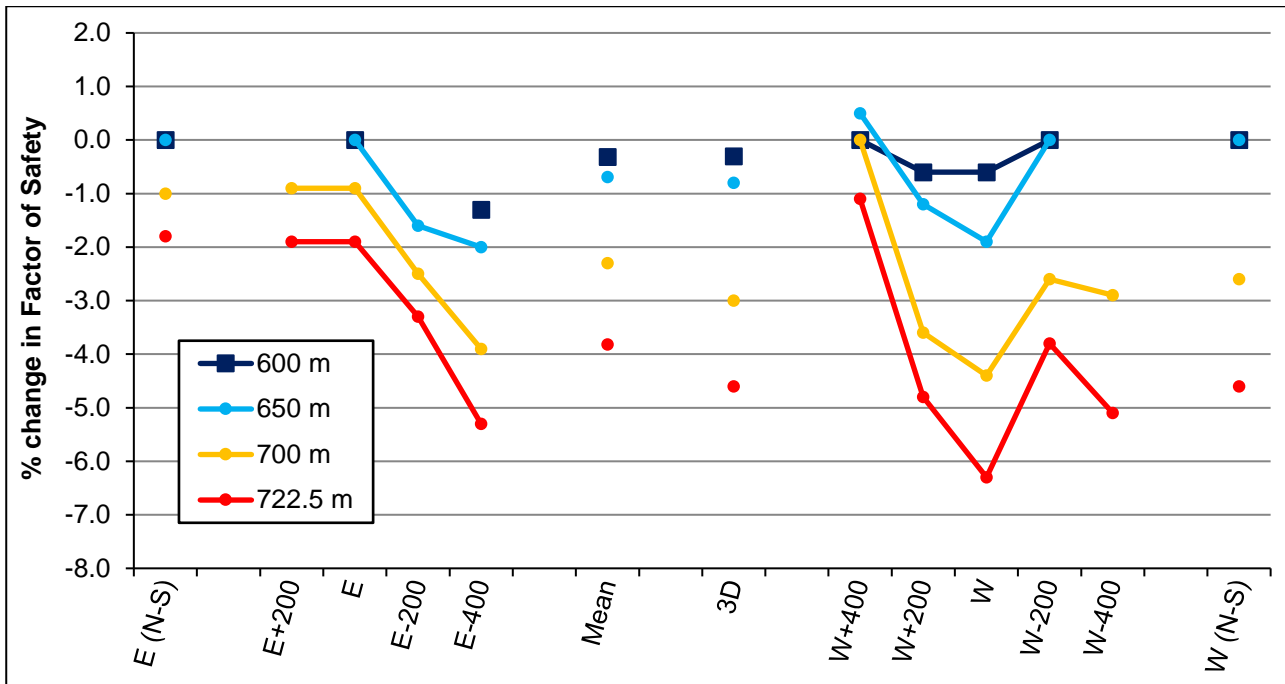


Figure 7. Changes in the Factor of Safety from the dry slope condition, obtained from all 2D and 3D analyses assuming mean unit weight = 23 kN m^{-3} , for water table elevations coinciding with four external reservoir levels. There are no results for some combinations as shown in Table 5.

Table 6. Results of the 3D analyses of the Vaiont landslide for various slope conditions with unit weight = 23 kN m^{-3} .

	Factor of Safety using $\phi' = 25^\circ$ throughout	% change from the dry slope FS
Dry slope	1.026	--
Reservoir at 600 m	1.023	-0.28
Reservoir at 650 m	1.018	-0.77
Reservoir at 700 m	0.995	-3.03
Reservoir at 722.5 m	0.978	-4.65

supporting load from the reservoir water was to reduce the overall FS of each cross-section profile as shown in Table 5 and Figs. 4 and 6. The greatest reduction in the FS corresponded in all cases with the highest water level analysed (i.e. the design reservoir level at 722.5 m). The same pattern of results was found for the 3D analyses of the entire landslide (Table 6). The critical pool level, above which the FS would have started to increase with higher water level due to the beneficial supporting effect of the reservoir water, was found by [Dedic \(1987\)](#) for a ‘chair’-shaped failure

surface to vary between around 740 m and over 800 m depending on antecedent rainfall (affecting artesian groundwater) and shear strength used for his 3D analyses. We have not determined this level for the actual failure surface but our results show that it was never going to be attained, being higher than the maximum possible reservoir elevation.

The reductions in FS (Fig. 7, which includes results from Table 6) are the maximum achievable for each water level elevation because the starting point is the limiting ‘least bad’ initial condition and does not include the effects of heavy rainfall. There will undoubtedly have been some pore water pressures within the slope for some of the time resulting in the FS being slightly less than the ‘dry slope’ case so that the reductions would be smaller in reality. For the same reason the mobilized friction angle along each of these profiles for FS = 1.0 must have exceeded that shown in Table 5 and Fig. 5, or for the entire landslide must have exceeded 24.4° overall.

The much smaller reduction in FS at profile W-200 appears to result from the much smaller extent of failure surface affected by the reservoir-induced groundwater relative to the large overall mass along this profile. Likewise, W+400 showed a small improvement in stability (+0.5%) at the end of the ‘first filling’ due to the very small zone of toe saturation to 650 m elevation compared with the greater external depth of inundation below 650 m.

4.3 Analysis of the pore pressure coefficient

The actual pore water pressures at the time of failure are unknown. Piezometers P1–P3 all showed a water table within the slope varying exactly with external reservoir level (Fig. 19 in Müller 1964), although this was always below Bistacchi et al.’s (2013) failure surface at P2 (Dykes and Bromhead – in press). The effect of this condition on the stability of the slope can be argued theoretically in order to further support our results using the pore pressure coefficient r_u , i.e. the ratio of the pore water pressure to the vertical stress due to the slope mass:

$$r_u = u / \gamma z$$

where γ is the unit weight of the slope mass, z is the thickness of the slope mass above the reference depth and u is the pore water pressure:

$$u = \gamma_w h$$

where γ_w is the unit weight of water and h is the water table height above the reference depth. If $\gamma = 20$ (or 23) kN m^{-3} and $\gamma_w = 10 \text{ kN m}^{-3}$, a piezometric line at ground level gives $r_u = 0.5$ (or 0.426). Therefore a piezometric line halfway up from the failure surface to the ground level gives $r_u = 0.25$

(or 0.213). Applying this idea to the northern slope of Mt Toc for an example condition to demonstrate the point, $r_u = 0.2$ would require a mean $\phi_p' = 38^\circ$ for stability, or $c' = 20\%$ of the average shear stress – possibly more than 200 kPa – or an intermediate combination of both. A higher water table giving a higher r_u would require even more extreme shear strength values for stability to be maintained. Of course, these theoretical conditions (Fig. 8) assume a water table between the failure surface and the ground surface throughout the full length of the landslide, whereas in reality only the lower part of the failure surface saw large local increases in r_u due to reservoir-induced groundwater. A much thinner perched water table further up the slope can be reasonably hypothesised, from previous arguments, in the absence of any relevant data. However, the argument for higher peak shear strengths than those in Table 5 and Fig. 6 is further reinforced.

Our results therefore demonstrate several key features of the Vaiont landslide:

1. Prior to 1960, the slope must have been controlled by peak friction angles throughout.
2. The available friction angles must have been significantly higher than our results indicate.
3. Limestone beds must have contributed to the available shear strength until the final failure.
4. Progressive failure may have been initiated in late 1960 by the extreme rainfall, the reservoir appearing to have an almost negligible effect on the Factor of Safety at that stage.

Furthermore, all significant accelerations of ground movement immediately followed periods of high rainfall, irrespective of reservoir levels, but the reservoir may have impeded drainage of perched groundwater that resulted from the rainfall.

5 Discussion

The results of routine ‘limit equilibrium’ stability analyses of the Vaiont landslide using the new failure surface geometry, combined with basic geotechnical principles, allow us to invoke Occam’s Razor in order to explain the entire event. The 1963 landslide was a first-time moderately translational dip-slope rockslide that was initiated by very high rainfall that happened to coincide with particular phases of reservoir filling, then developed by progressive failure of thin clay layers. When enough of the available shear strength in the slope had been reduced from peak to residual, a process possibly accelerated by the supposed effect of reservoir water impeding drainage of further very high rainfall, the remaining intact rock failed catastrophically and the entire mass was able to accelerate and achieve the observed displacement within the estimated 30-45 s. No other mechanisms are required and all observed and recorded evidence relating to the site and the event can be accounted for (Dykes and Bromhead – in press).

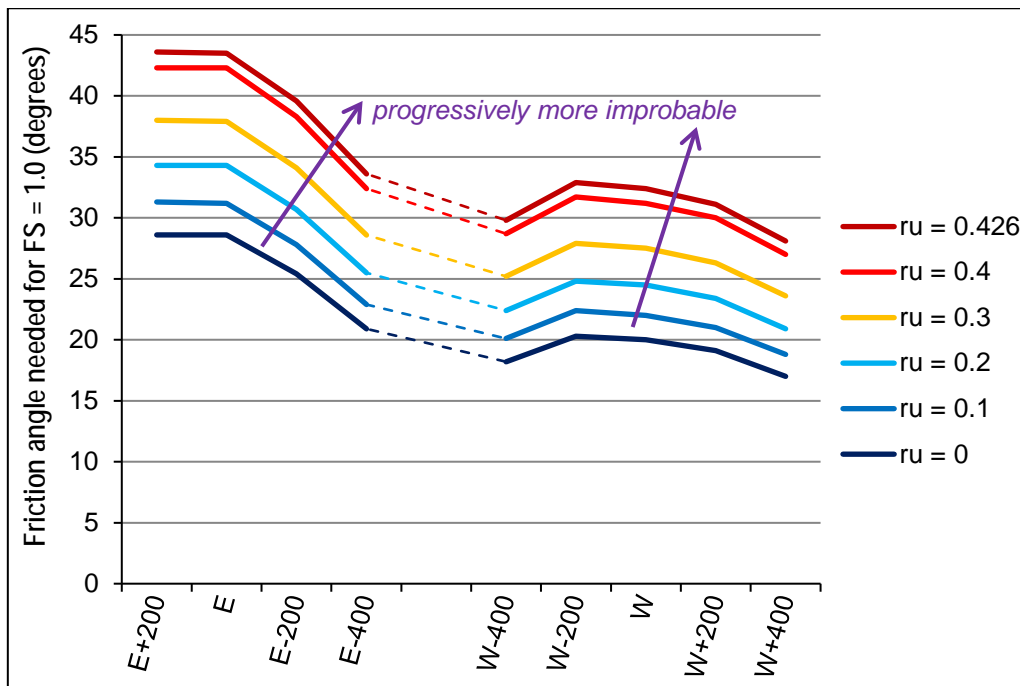


Figure 8. Mobilised friction angles (assuming $c' = 0$) for hypothetical pore water pressure conditions defined by the pore pressure ratio ($'ru' = r_u$) from $r_u = 0$ (dry slope condition) to $r_u = 0.426$ (water table at the ground surface for $\gamma = 23 \text{ kN m}^{-3}$).

5.1 Ground model

The importance of an accurate ground model for any proposed engineering project cannot be overstated. The new model of the failure surface shows a gently curving bowl-shaped surface in 3D. This overall form had been suggested as early as 1964 though with more angular transitions between different segments of the surface (Broili 1967). However, cross-sections drawn in the assumed direction of movement tended to show the characteristic ‘chair’ shape of the failure surface that formed the basis of many of the attempts to explain the landslide over subsequent decades. The new cross-sections (Bistacchi et al. 2013) show some convexity of the shear surface between the upper and lower parts but as a gentle arc and not a tight ‘hinge’ (Fig. 4). Furthermore, the shear surface always has at least a moderate gradient towards the gorge – and there is no ‘chair’. This validates element H3 of our hypothesis (Table 1). This failure surface geometry, combined with evidence of the shear strength needing to be at its peak (intact) value prior to the landslide (Section 5.2), can account for the observed rapid acceleration of the landslide. Cross-sections with these characteristics had been presented by Kiersch (1964) but were strongly argued to be incorrect by

Müller (1968). Consequently such details, and particularly the three-dimensional characteristics of the failure surface, may have been overlooked during later investigations.

5.2 Stability analyses

The results of our new stability analyses lead to several fundamental revisions of our understanding of the 1963 landslide. An overall friction angle of $\phi_p' > 24^\circ$ is needed for stability ($FS \geq 1.0$) so the mountain slope could not have remained in place prior to 1963 if there was an old failure surface at residual strength. Therefore the landslide was not a reactivation of an ancient landslide, which necessarily means that most of the northern side of Mt Toc comprised intact in-situ rock prior to this event. This is consistent with explanations of the development of the landslide in terms of fracture propagation (Havaej et al. 2015) including within clays at high confining stresses (Kilburn and Petley 2003) and taking account of the geological conditions generally throughout the rock mass (Wolter et al. 2014). It also validates elements H1 and H2 of our hypothesis (Table 1). Belloni and Stefani (1992) highlighted Caloi's (1966) seismic results as indicating essentially 'in situ rock' in 1959 with a deterioration in the quality of the rock mass between 1959 and 1960 due to 'fracturing processes in the deeper lying rock layers' (Müller 1964, p.168). This is also consistent with the accounts cited above.

Our interpretations are based on minimum shear strengths, represented as friction angles, for a completely dry slope, so our arguments are reinforced by the need for these to have been higher in reality due to any water in the slope. Table 5 suggests that the clay alone could have controlled the stability of the western side of the landslide, given that the clay layers with relatively high montmorillonite contents (Hendron and Patton 1985) and very high confining stresses (Kilburn and Petley 2003), probably had peak friction angles around $\phi_p' = 22\text{--}26^\circ$. Table 5 and Fig. 5 also show that a much higher friction angle was required for stability of the steeper eastern side of the landslide, but there was significantly higher resistance towards the eastern margin due to the failure surface having to rise through the limestone beds. Hendron and Patton (1985) suggested $\phi_p' = 36^\circ$ for this zone, corresponding with friction along limestone joints. Therefore, the minimum overall friction angle of $\phi_p' = 24.4^\circ$ obtained from the first 3D analysis must have been higher in reality, and individual 2D profiles must have had more strength than indicated. The observed movements of the slope indicated a coherent rigid mass above developing shear surfaces, which means that the limestone beds were providing a significant proportion of the overall strength. The expected 50% reduction in the FS corresponding with the halving of the friction angle from $\phi_p' = 25^\circ$ to $\phi_r' = 12^\circ$,

given that the driving force is constant, was found from a further 3D analysis. It is the sudden loss of the final elements of peak strength, probably closer to the (lower) eastern margin, that ‘released’ the slope and allowed it to accelerate.

5.3 Groundwater trigger

Movements of the northern slope of Mt Toc began in late September 1960 during the ‘first filling’ of the reservoir (February to November), which coincided with a period of unusually wet weather (June to October). In late October 1960 (reservoir level 645 m), a 2 km long crack was discovered that defined the exact outline of the eventual landslide. Filling continued until the 700,000 m³ landslide of 4 November 1960 occurred, at which time the reservoir level (650 m) was below the toe of this landslide (Semenza 2001, 2010). During 1-4 November 1960 the rate of movement of the whole slope reduced, despite the increasing reservoir level, because it had stopped raining (Müller 1964; Hendron and Patton 1985). Hydrostatic water pressures due to the impoundment were not significantly affecting the stability, as shown also by the negligible FS reductions (mean < 1.0%) at 650 m water level (Figs. 6, 7; Table 6). The piezometer data (Müller 1964) show a water table at least 20 m below the failure surface, meaning that the landslide mass was underdrained and not subjected to artesian pressures from below (Dykes and Bromhead – in press). We therefore conclude that raised pore water pressures within the landslide mass due to the exceptional rainfall (including 425 mm in October 1960: Müller 1964) probably initiated the progressive failure leading to the 1963 landslide.

There are unfortunately no data that show any groundwater conditions within the landslide mass. Field observations and borehole cores indicated high overall permeabilities for the limestones above and below the failure surface (Hendron and Patton 1985; Semenza 2001, 2010) which allowed reservoir water to saturate the entire slope to the external water level with minimal lag. This was demonstrated clearly in the data once this level exceeded the natural water table elevation at each piezometer. Such rapid responses at three locations across the slope indicate a rising (or falling) horizontal water table throughout, as assumed for this study. However, the extent, continuity and hydrological influence of any clay layer(s) above the failure surface (see Section 2) is unknown.

The ‘second filling’ of the reservoir, following construction of a by-pass tunnel for any water trapped upstream of a possible landslide, started in October 1961 and continued until a significant acceleration of ground movements was observed at the start of November 1962. Filling of the reservoir was halted and the level was allowed to fall from its peak of 700 m; the rate of ground

movement steadily reduced concurrently. During late October/early November 1962, rainfall of around 120 mm in ten days was followed by around 240 mm within the next ten days. Piezometer P2, furthest upslope, showed a 10 m piezometric rise above the reservoir level but even this peaked around 15 m below the failure surface (Dykes and Bromhead – in press). This demonstrates the possibility of a significant perched water table forming above the failure surface from the same rainfall, promoting the accelerated movement into December 1962.

The final acceleration of the landslide commenced in early August 1963, immediately following around 200 mm of rain within ten days. Further high rainfall (>100 mm in each of the next two 10-day periods) must have generated further raised pore pressures from accumulated perched groundwater. The final failure was therefore probably not caused directly by the filling of the reservoir, but by the presence of the reservoir impeding natural drainage of the perched groundwater. Tables 5 and 6 and Figs. 5-7 demonstrate the very small influence of the reservoir on the overall stability of the slope. The reduction in the FS must have been less than 4.6% (Fig. 7) based on the 3D analyses because the slope probably contained some groundwater initially. Furthermore, Kilburn and Petley (2003) showed that this final 60-day phase of acceleration almost perfectly demonstrated the ‘Saito effect’ (Saito 1965) of a linear decrease in the inverse-deformation rate for progressive failures developing by brittle crack formation. These observations and interpretations support element H4 of our hypothesis (Table 1), although further modelling investigations of possible groundwater configurations are required.

5.4 Secondary failures

Pore water pressure distributions associated with a near-horizontal water table at the same elevation as the reservoir surface could allow the main mass to tear away from the two heads of the ‘M’ shape, a scenario impossible if the failure surface had a ‘chair’ shape (Fig. 2). Semenza (2001, 2010) highlighted a large mass that slid from the head of the east side and over-ran the main landslide deposit by up to 100 m. This mass, identified as the ‘eastern lobe’, retained its forest cover and therefore must have fallen after the flood wave had subsided. Wolter et al. (2016) showed that similar but smaller masses had likewise slipped from the head of the west side and retained their trees intact, consistent with a single photograph in the Vaiont-focused tourist visitor centre in Erto that shows a more pronounced head scarp above the west side in daylight (i.e. not earlier than the morning of 10 October). This duplicate evidence of retrogressive secondary failures some time after the main landslide further demonstrates the impossibility of a ‘chair’ shaped failure surface (Fig. 2) and is consistent with the more translational ground model discussed in this paper.

5.5 Vaiont landslide explained

Once the Vaiont gorge had been cut by glacial meltwater by the early Holocene, some form of large scale slope failure was inevitable. The Vaiont reservoir project may have very slightly accelerated the onset of a particularly large failure of the northern slope of Mt Toc. Indeed, we have discussed evidence of past landslides within or adjacent to the gorge, at least one of which blocked the lower part of the gorge causing it to fill up with alluvial sediment before a further landslide, triggered by rapid slope undercutting, deposited the mass of rock known as the ‘Colle Isolato’ on top of the infilled channel sediments (Dykes and Bromhead – in press; Wolter et al. 2016).

Filling of the reservoir commenced in February 1960 and the water level had reached almost 650 m by November 1960. Raised pore water pressures within the slope above the Fonzaso Formation clay layers, due to percolation of exceptionally high rainfall – possibly exacerbated very slightly by reservoir impoundment effects (Hendron and Patton 1985) – caused the initiation of progressive failure within the mountain. The ‘M’-shaped crack was discovered and monitoring was initiated in October, and although no part of the 4 November landslide was ever influenced by the reservoir (Semenza 2001, 2010), filling was stopped.

In these early stages, localised ‘brittle’ crack initiation and propagation within clay layers commenced (Kilburn and Petley 2003; Havaej et al. 2015) with any initial displacements being taken up by differential movement of limestone beds along or against existing joints. As cracking and micro-shearing within the clays progressed, the available shear strength started to fall locally, mobilising additional shear strength in adjacent parts of the mass. The November 1960 rockslide may have allowed new stress relief joints to form but had little tangible effect on the overall stability of Mt Toc.

During the ‘first filling’ of the reservoir during 1960, the largest velocities were recorded in the lower west side of the slope, with movements above the Pozza being lower by about half. Velocities were lower still in the upper east side, reducing towards the gorge east of the Massalezza Ditch (Müller 1964). This pattern is consistent with a down-dip (i.e. ENE) vector of shear stress on the failure surface modifying the downslope trend, in which the lower west side is entirely unsupported but the lower east side is supported and resisted by the great thickness of intact beds stratigraphically above the failure surface. This eastern margin of the unstable mass was therefore affected by some component of compressive as well as shear stresses.

Rainfall fell to more normal levels as the reservoir level was reduced to allow the bypass tunnel to be built, and movement of the entire mountainside stopped. During the 'second' filling of the reservoir, rainfall was normal and measured ground movements were of the order of 1-2 mm d⁻¹. Although extremely low, continuing movements suggest ongoing weakening of the clay layers, probably independently of water conditions. Furthermore, the development of cracks within, and probably through, the clay layers must have increased the overall permeability of the mass, allowing enhanced percolation of groundwater between adjacent fractured limestone beds. The unstable mass did not accelerate significantly until another period of exceptional rainfall around early November 1962, at which point the reservoir may have impeded drainage of the new perched groundwater to prolong the existence of raised pore water pressures up-dip of the reservoir-induced groundwater. The final acceleration during the 'third filling', starting in August 1963 and continuing to the failure, is likely to have involved the same general condition.

As the strength was progressively lost from the clay layers (Kilburn and Petley 2003), the limestone rock-bridges (Sturzenegger and Stead 2012) provided more of the mobilised strength in the final period of acceleration prior to the landslide, particularly near the eastern margin. Indeed, Delle Rose (2012) reported Caloi's (1966) interpretation of seismicity within the northern slope of Mt Toc generally migrating eastwards during the 1960-63 monitoring period, again consistent with the observed pattern of movement and with the structural explanation for this. At some stage, enough of the clay layers had formed shear surfaces with friction angles reduced to residual ($\phi_r' = 8-12^\circ$: Tika and Hutchinson (1999) measured 10°), and enough additional cracks had formed through previously intact limestone beds, that there was insufficient strength in the remaining rock-bridges to resist further movement of the mass. Hence, on 9 October 1963, brittle failure of limestone beds, particularly those along the eastern margin, occurred. This led to an extremely rapid loss of strength from peak (limestone) to residual (montmorillonite-rich clay), allowing the observed rapid acceleration and large displacement of over 240 million m³ of rock, effectively as a single unit but with around 5° of convergence between the west side (360 m displacement) and the east side (460 m, overriding part of the west side mass near the toe) (Bistacchi et al. 2013).

Several studies suggested that heating of pore water due to the friction generated by the movement could have reduced ϕ_r' further and contributed to the acceleration (e.g. Voight and Faust 1982; Nonveiller 1992; Pinyol and Alonso 2010). We agree with Kilburn and Petley (2003) that this effect is not necessary to account for the failure characteristics but that we also do not exclude the possibility that it may have occurred to some degree. The effects of the displaced water from the reservoir are well documented elsewhere. Retrogressive development of the heads of both sides of the landslide occurred following subsidence of the flood.

6 Conclusions

The Vaiont landslide was a very large first-time moderately translational bedding-controlled (dip-slope) landslide that resulted from the geological consequences of a complex tectonic history followed by a geologically extremely rapid removal of toe support due to the Vaiont Gorge being formed. It did not have a ‘chair’-shaped failure surface. It was probably initiated by the very high rainfall that happened to coincide with the first reservoir filling and then developed by progressive failure of thin clay layers. The progressive failure process was accelerated by subsequent periods of very high rainfall, the perched groundwater from which could not easily drain from the slope due to reservoir water. When enough of the slope had been reduced from peak to residual shear strength, the remainder failed rapidly and the entire mass was able to accelerate and achieve the observed displacement within the estimated 30-45 s.

The key to understanding the Vaiont landslide is the failure surface geometry, which was controlled by the structural geology. We have taken new findings from Vaiont by [Bistacchi et al. \(2013\)](#) and synthesised them with the findings of previous studies of the landslide to provide an explanation of the landslide that is both simple, consistent with known details and can account for its occurrence *and* behaviour – *and* all of the other contemporary observations and evidence. We used zero pore water pressures as the reference pre-failure slope condition because if there had been any pore pressures then the conclusions of our analyses would have been even stronger. Submergence provides the same support to the toe slope whether the failure surface is ‘chair’-shaped or not, but the pore pressure increase is much less without a ‘chair’ because the length of affected slip surface and the mean water table height above it are significantly smaller. Thus, if the destabilising effect of the pore water pressure on the failure surface is less than [Hendron and Patton \(1985\)](#) assumed for their analyses using a ‘chair’ shape, then it reinforces their view (consistent with our own) that the rainfall was a primary factor in the disaster.

This account demonstrates that there was nothing special about the Vaiont landslide compared with any other large dip-slope rockslides except perhaps the juxtaposition of an unusual underlying geological structure with a rather spectacular geomorphological context. It is to be expected that such features and any associated risks, including from deep groundwater circulation patterns, would be more accurately identified from modern site investigations, largely as a result of what happened at Vaiont. In other words, it is critical that geologists, geomorphologists and geotechnical engineers work together to make sure that a ground model is correct before starting a project. Finally, Vaiont

falls entirely within the scope of current knowledge and can no longer be disregarded from hazard and risk studies on the grounds of being a ‘special case’ or otherwise ‘inexplicable’.

Acknowledgements

We thank the reviewers for their particularly detailed comments which have ultimately contributed to the robustness of this paper.

References

- Alonso EE, Pinyol NM (2010) Criteria for rapid sliding I. A review of Vaiont case. *Engineering Geology* 114, 198-210.
- Anderson DL (1985) Appendix B: Static slope analysis method used for the Vaiont slide analysis. In Hendron and Patton: The Vaiont slide, a geotechnical analysis based on new geologic observations of the failure surface. US Army Corps of Engineering Technical Report GL-85-5, Volume 2, B1-B8. Available at: www.dtic.mil/dtic/tr/fulltext/u2/a158193.pdf (accessed 22 April 2017).
- Belloni LG, Stefani RF (1992) Natural and induced seismicity at the Vajont slide. In Semenza E, Melidoro G (eds) Proc. Meeting on the 1963 Vaiont Landslide, Ferrara 1986. University of Ferrara, Ferrara, 115-132.
- Bishop AW (1955) The use of the slip circle in the stability analysis of slopes. *Géotechnique* 5, 7-17.
- Bistacchi A, Massironi M, Superchi L, Zorzi L, Francese R, Giorgi M, Chistolini F, Genevois R (2013) A 3D geological model of the 1963 Vajont landslide. In Genevois R, Prestininzi A (eds) International Conference on Vajont – 1963-2013: Thoughts and analyses after 50 years since the catastrophic landslide. Italian Journal of Engineering Geology and Environment – Book Series No.6. Sapienza Università Editrice, Rome, 531-539.
- BRE (1997) Technical Data Sheet: Portland Base Bed Limestone. Building Research Establishment, Watford. Available at: <http://projects.bre.co.uk/ConDiv/stonelist/portfancybase.html> (accessed 20 April 2017).
- Broili L (1967) New knowledges on the geomorphology of the Vaiont slide slip surfaces. *Rock Mechanics and Engineering Geology* 5, 38-88.
- Bromhead EN (2004) Landslide slip surfaces: their origins, behaviour and geometry. Keynote paper. Proceedings, 9th International Symposium on Landslides, Rio de Janeiro. Balkema, Amsterdam, Vol. 1, 3-22.
- Bromhead EN, Harris AJ, Watson PDJ (1999) Influence of pore water pressures in partly submerged slopes on the critical pool level. Symposium on Landslides, IS-SHIKOKU November 1999, 411-416.
- Caloi P (1966) L’evento del Vajont nei suoi aspetti geodinamici. *Annals of Geophysics* 19, 1-87. (in Italian)
- Chandler RJ (1977) Back analysis techniques for slope stabilization works: A case record. *Géotechnique* 27, 479-495.

- Crosta GB, Imposimato S, Roddeman D (2016) Landslide spreading, impulse water waves and modelling of the Vajont rockslide. *Rock Mechanics and Rock Engineering* 49, 2413-2436.
- Dedic M (1987) A back-analysis of the Vaiont slide based on recent geological data. Unpublished MSc thesis, Imperial College, University of London.
- Delle Rose M (2012) Some insights about the relation among seismic activity, tectonic structures and rockslide kinematics at the Vajont dam site. In: Proceedings, 31 Convegno Nazionale, Gruppo Nazionale di Geofisica della Terra Solida (GNGTS), Potenza, Italy, 44-50.
- Del Ventisette C, Gigli G, Bonini M, Corti G, Montanari D, Santoro S, Sani F, Fanti R, Casagli N (2015) Insights from analogue modelling into the deformation mechanism of the Vaiont landslide. *Geomorphology* 228, 52-59.
- De Mello VFM, Larocca ES, Quintanilha R, de Meireles EB (2004) Reappraising historical coincidences that radically misled slope destabilization analyses of homogeneous earth dams. In: *Advances in Geotechnical Engineering: The Skempton Conference (ICE)*, London, March 2004, Vol. 2, 881-897.
- Doveton JH (1999) *Basics of Oil and Gas Log Analysis*. Kansas Geological Survey (University of Kansas), Lawrence. Available at: www.kgs.ku.edu/PRS/Info/pdf/doveton2.PDF (accessed 20 April 2017).
- Dykes AP, Bromhead EN (in press) The Vaiont landslide: Re-assessment of the evidence leads to rejection of the consensus. To be published in *Landslides* – awaiting final acceptance.
- Genevois R, Prestininzi A (eds) (2013) *International Conference on Vajont – 1963-2013: Thoughts and analyses after 50 years since the catastrophic landslide*. Italian Journal of Engineering Geology and Environment – Book Series No.6. Sapienza Università Editrice, Rome.
- Ghirotti M, Masetti D, Massironi M, Oddone E, Sapigni M, Zampieri D, Wolter A (2013) The 1963 Vajont landslide (Northeast Alps, Italy): Post-conference field trip (October 10th, 2013). In Genevois R, Prestininzi A (eds) *International Conference on Vajont – 1963-2013: Thoughts and analyses after 50 years since the catastrophic landslide*. Italian Journal of Engineering Geology and Environment – Book Series No.6. Sapienza Università Editrice, Rome, 635-646.
- Havaej M, Wolter A, Stead D (2015) The possible role of brittle rock fracture in the 1963 Vajont Slide, Italy. *International Journal of Rock Mechanics and Mining Sciences* 78, 319-330.
- Hendron AJ, Patton FD (1985) *The Vaiont slide, a geotechnical analysis based on new geologic observations of the failure surface*. US Army Corps of Engineering Technical Report GL-85-5 (2 volumes). Available at: www.dtic.mil/dtic/tr/fulltext/u2/a158192.pdf (Vol. 1), www.dtic.mil/dtic/tr/fulltext/u2/a158193.pdf (Vol. 2) (accessed 22 April 2017).
- Hungr O (1987) An extension of Bishop's simplified method of slope stability analysis to three dimensions. *Géotechnique* 37, 113-117.
- Hungr O (1989) Evaluation of a Three-dimensional method of slope stability analysis. *Canadian Geotechnical Journal* 26, 679-686.
- Hutchinson JN (1969) A reconsideration of the coastal landslides at Folkestone Warren, Kent. *Géotechnique* 19, 6-38.

- Kiersch GA (1964) Vaiont reservoir disaster: Geologic causes of tremendous landslide accompanied by destructive flood wave. *Civil Engineering (The Magazine of Engineered Construction)*, March 1964, 32-39.
- Kilburn CRJ, Petley DN (2003) Forecasting giant, catastrophic slope collapse: lessons from Vajont, Northern Italy. *Geomorphology* 54, 21-32.
- Manger GE (1963) Porosity and Bulk Density of Sedimentary Rocks. *Contributions to Geochemistry: Geological Survey Bulletin 1144-E*. United States Department of the Interior, Washington D.C.. Available at: <https://pubs.usgs.gov/bul/1144e/report.pdf> (accessed 20 April 2017).
- Martinis B (1978) Contributo alla stratigrafia dei dintorni di Erto-Casso (Pordenone) e dalla conoscenza delle caratteristiche strutturali e meccaniche della frana del Vajont. *Memorie di Scienze Geologiche Università di Padova* 32, 1-33. (in Italian)
- Masè G, Semenza M, Semenza Paolo, Semenza Pietro, Turrini MC (Eds.) (2004) *Le foto della frana del Vajont. La scoperta dell'antica frana – Le fotografie e gli studi geologici di Edoardo Semenza, Franco Guidici and Daniele Rossi prima e dopo la catastrofe del 9 ottobre 1963 Volume and CD-ROM*. K-flash, Ferrara.
- Massironi M, Zampieri D, Superchi L, Bistacchi A, Ravagnan R, Bergamo A, Ghirotti M, Genevois R (2013) Geological structures of the Vajont landslide. In Genevois R, Prestininzi A (eds) *International Conference on Vajont – 1963-2013: Thoughts and analyses after 50 years since the catastrophic landslide*. *Italian Journal of Engineering Geology and Environment – Book Series No.6*. Sapienza Università Editrice, Rome, 573-582.
- Müller L (1964) The rock slide in the Vajont valley. *Rock Mechanics and Engineering Geology* 2, 148-212.
- Müller L (1968) New considerations on the Vaiont slide. *Rock Mechanics and Engineering Geology* 6, 1-91.
- NCS (2017) *Materials: Limestone*. Natural Cut Stone Ltd., Nottingham. Available at: <http://naturalcutstone.co.uk/materials/limestone-materials/> (accessed 20 April 2017).
- Nonveiller E (1992) Vaiont slide – Influence of frictional heat on slip velocity. In Semenza E, Melidoro G (eds) *Proc. Meeting on the 1963 Vaiont Landslide, Ferrara 1986*. University of Ferrara, Ferrara, 187-197.
- Paronuzzi P, Bolla A (2012) The prehistoric Vajont rockslide: An updated geological model. *Geomorphology* 169-170, 165-191.
- Pinyol NM, Alonso EE (2010) Criteria for rapid sliding II. Thermo-hydro-mechanical and scale effects in Vaiont case. *Engineering Geology* 114, 211-227.
- Romero SU, Molina R (1974) Kinematic aspects of Vaiont slide. *Proceedings of the 3rd Congress ISRM, Denver, Colorado, Vol. 2*, 865-870.
- Rossi D, Semenza E (1965) *Carte geologiche del versante settentrionale del M. Toc e zone limitrofe, prima e dopo il fenomeno di scivolamento del 9 ottobre 1963, Scala 1:5000*. Istituto di Geologia, Università di Ferrara, 2 maps.
- Saito M (1965) Forecasting the time of occurrence of a slope failure. *Proceedings of the 6th International Conference on Soil Mechanics and Foundation Engineering* 2, 537-541.

- Semenza E (2001) *La Storia del Vaiont raccontata dal geologo che ha scoperto la frana*. Tecomproject Editore, Ferrara. (in Italian)
- Semenza E (2010) *The Story of Vaiont Told by the Geologist Who Discovered the Landslide*. Translation by Carolyn Goodman Masè of Semenza (2001). K-flash, Ferrara.
- Skempton AW (1948) The rate of softening in stiff-fissured clays, with special reference to London clay. Proc. 2nd International Conference on Soil Mechanics and Foundation Engineering, Vol. 2, 50-53.
- Sturzenegger M, Stead D (2012) The Palliser Rockslide, Canadian Rocky Mountains: characterization and modeling of a stepped failure surface. *Geomorphology* 138, 145-161.
- Superchi L (2012) *The Vajont rockslide: new techniques and traditional methods to re-evaluate the catastrophic event*. Unpublished PhD thesis, Università degli Studi di Padova, Padova, Italy.
- Tika Th E, Hutchinson JN (1999) Ring shear tests on soil from the Vaiont landslide slip surface. *Géotechnique* 49, 59-74.
- Voight B, Faust C (1982) Frictional heat and strength loss in some rapid landslides. *Geotechnique* 52, 157-171.
- Wolter A, Stead D, Clague JJ (2014) A morphologic characterisation of the 1963 Vajont Slide, Italy, using long-range terrestrial photogrammetry. *Geomorphology* 206, 147-164.
- Wolter A, Stead D, Ward BC, Clague JJ, Ghirotti M (2016) Engineering geomorphological characterisation of the Vajont slide, Italy, and a new interpretation of the chronology and evolution of the landslide. *Landslides* 13, 1067-1081.

Tables

Table 1. Elements of the established consensus and the new hypothesis relating to the Vaiont landslide, showing reference codes used in this paper (from Dykes and Bromhead – in press).

Ref.	Element of the consensus	Ref.	Element of the new hypothesis
C1	the failure was a reactivation of an ancient landslide	H1	the 1963 landslide was a first-time failure
C2	both the prehistoric landslide and the 1963 landslide took place along thin clay seams in a limestone mass and that these were at, or near, residual strength prior to 1960	H2	failure took place along thin clay seams in a limestone mass that were initially at peak strength prior to 1960
C3	the shape of the sliding surface followed a folded rock structure that comprised a subhorizontal lower part and a steeply inclined upper part, commonly referred to in the literature as a ‘chair’ shape	H3	the sliding surface did not have a ‘chair’ shape but was moderately translational
C4	the trigger for the reactivation was a major loss in stability due to impounding of the reservoir and inundation of the toe of the slide mass	H4	failure was triggered by inundation of the toe of the slide mass coinciding with heavy rainfall, such that the reservoir may not have been necessary to bring about failure

Table 2. Indicative stratigraphy of the south side of the Vaiont valley (after Bistacchi et al. 2013 and Ghirotti et al. 2013).

Age	Stratigraphy	Thickness
Paleocene	Scaglia Rossa	~300 m
Upper Cretaceous		
Cretaceous	Calcere di Socchèr (or ‘Biancone Formation’)	150 m
Upper Jurassic	Rosso Ammonitico	0–15 m
	Fonzaso Formation	10-40 m
Middle Jurassic	Vajont Limestone	350–450 m

Table 3. Published densities and unit weights assumed to apply to the Vaiont landslide at the time of failure.

Unit Weight (kN m ⁻³)	Reference
26 (relative density = 2.65)	Martinis (1978)
26.5 (relative density = 2.7)	Anderson (1985)
23.5	Alonso and Pinyol (2010)
26.3 – 26.5	Superchi (2012)
24.5	Ventisette et al. (2015)

Table 4. Derived unit weights of some Mesozoic limestones and dolostones (n.s. = not stated).

Limestone Formation	Dry – Saturated Unit Weight (kN m⁻³)	Reference
Triassic		
Thaynes Limestone, Wyoming, USA	26.0 – 26.1	Manger (1963)
Ross Fork Limestone, Wyoming, USA	24.7 – 25.4	
Muschelkalk, Mutzig, Germany	26.3 – 26.4	
Muschelkalk, Galicia, Poland	24.1 – 25.4	
Limestone (part dolomitic), Switzerland	26.2 – 26.5	
Marble, Switzerland	25.9 – 26.2	
Jurassic		
Twin Creek Limestone, Wyoming, USA	27.0 – 27.0	Manger (1963)
Carmel formation (limestone), Utah, USA	26.0 – 26.2	
Solenhofen Limestone, Germany	25.2 – 25.6	
Limestone, Switzerland	25.8 – 26.1 25.2 – 25.8	
Inferior oolite, England	22.9 – 24.1	
Oolite, England	22.1 – 23.6	
White Lias, England	23.9 – 24.8	
Oolitic Jurassic limestone, England (various different named quarried beds)	20.7-23.6 – not stated	NCS (2017)
Oolitic Bioclastic limestone, England	18.0 – n.s. 19.6 – n.s.	
Middle Jurassic Oolitic Limestone from the Bath Oolite Horizon, England	19.5 – n.s. 20.9 – n.s.	
Portland limestone, England	24.9 – 25.8	
Portland Base Bed limestone, England	21.0 – n.s.	BRE (1997)
Cretaceous		
Caddo limestone, Texas, USA	25.3 – 25.7	Manger (1963)
Glen Rose Limestone, Texas, USA	21.7 – 23.2	
Peterson Limestone, Wyoming, USA	24.0 – 24.9	
Limestone, Switzerland	25.5 – 26.0	
MEAN:	23.5 – 25.6	

Table 5. Results of 2D stability analyses of cross-sections through the Vaiont landslide (Figs. 4, 5) for a various slope conditions with unit weight = 23 kN m⁻³. Profiles E (N-S) and W (N-S) are the north-south versions of E and W.

Profile:	W (N-S)	W-400	W-200	W ¹	W+200	W+400	E-400	E-200	E ¹	E+200	E (N-S)
	Normal effective stress (kPa):										
Dry slope	2294	1457	2281	2501	2596	2376	2560	2160	1910	1095	2001
Reservoir at 600 m	2292	²	2277	2475	2541	2353	2519	²	1902	²	2001
Reservoir at 650 m	2267	²	2246	2401	2457	2294	2449	2083	1880	²	1987
Reservoir at 700 m	2159	1374	2139	2267	2301	2154	2322	2008	1830	1073	1947
Reservoir at 722.5 m	2092	1316	2072	2193	2217	2063	2248	1961	1800	1057	1918
Reservoir at 725 m	2084	1309	2064	2185	2207	2053	2240	1956	1796	1055	1915
	Shear stress (kPa):										
Dry slope	865	479	845	910	898	727	975	1025	1041	598	1042
Reservoir at 600 m	864	²	844	906	884	719	968	²	1037	²	1042
Reservoir at 650 m	854	²	832	891	860	697	949	1000	1027	²	1036
Reservoir at 700 m	836	468	811	864	825	660	918	976	1007	593	1023
Reservoir at 722.5 m	825	458	798	848	807	638	900	963	996	587	1014
Reservoir at 725 m	823	456	796	846	805	636	898	961	995	586	1013
	Angle of internal friction, ϕ' , for FS = 1.0:										
Dry slope	20.7°	18.2°	20.3°	20.0°	19.1°	17.0°	20.9°	25.4°	28.6°	28.7°	27.5°
Reservoir at 600 m	20.7°	²	20.3°	20.1°	19.2°	17.0°	21.0°	²	28.6°	²	27.5°
Reservoir at 650 m	20.6°	²	20.3°	20.4°	19.3°	16.9°	21.2°	25.6°	28.7°	²	27.5°
Reservoir at 700 m	21.2°	18.8°	20.8°	20.9°	19.7°	17.0°	21.6°	26.0°	28.8°	28.9°	27.7°
Reservoir at 722.5 m	21.5°	19.2°	21.1°	21.1°	20.0°	17.2°	21.8°	26.2°	29.0°	29.0°	27.9°
Reservoir at 725 m	21.6°	19.2°	21.1°	21.2°	20.0°	17.2°	21.8°	26.2°	29.0°	29.1°	27.9°
	Factor of Safety using $\phi' = 30^\circ$ throughout:										
Dry slope	1.53	1.75	1.56	1.59	1.67	1.89	1.52	1.22	1.06	1.06	1.11
Reservoir at 600 m	1.53	²	1.56	1.58	1.66	1.89	1.50	²	1.06	²	1.11
Reservoir at 650 m	1.53	²	1.56	1.56	1.65	1.90	1.49	1.20	1.06	²	1.11
Reservoir at 700 m	1.49	1.70	1.52	1.52	1.61	1.89	1.46	1.19	1.05	1.05	1.10
Reservoir at 722.5 m	1.46	1.66	1.50	1.49	1.59	1.87	1.44	1.18	1.04	1.04	1.09
Reservoir at 725 m	1.46	1.66	1.50	1.49	1.58	1.86	1.44	1.17	1.04	1.04	1.09

Notes

¹ Profile presented by Bistacchi et al. (2013)

² Failure surface always above this level or (at E-200 m) with negligible inundated mass at this level

List of Figures

Figure 1. Location of Longarone and the Vaiont landslide north of Venice (Venezia) in northern Italy.

Figure 2. Slope stability principles that negate the ‘chair’ hypothesis. (A) Simple representation of the problem with a ‘chair’ structure. (B) Internal and external changes affecting a hypothetical ‘chair’-shaped landslide. (C) Loss of driving force if the upper part of Block 2 is not included. (D) Simple representation of how the local Factor of Safety varies along a translational landslide.

Figure 3. Failure surface map with x - y axes in metres and contours at 50 m intervals, showing lines of cross-sections analysed in this paper. The light blue line is E (N-S) and the orange line is W (N-S). Failure surface contours and Sections ‘E’ and ‘W’ after Bistacchi et al. (2013).

Figure 4. Analysed 2D slope profiles through the Vaiont landslide (Fig. 3). Reservoir and groundwater elevations of 650 m and 722.5 m are shown for each profile. The approximate position of the 1960 landslide (dashed line) is indicated on profiles W and W-200.

Figure 5. Mobilised friction angle ($c' = 0$) to maintain stability of each 2D profile for different unit weight assumptions ($\gamma = \gamma$, kN m^{-3}) under completely dry and maximum inundation water table conditions.

Figure 6. Reductions in the Factor of Safety from the dry slope condition at each 2D profile arising from different unit weight assumptions ($\gamma = \gamma$, kN m^{-3}) for ‘first filling’ and maximum inundation water table elevations.

Figure 7. Changes in the Factor of Safety from the dry slope condition, obtained from all 2D and 3D analyses assuming mean unit weight = 23 kN m^{-3} , for water table elevations coinciding with four external reservoir levels. There are no results for some combinations as shown in Table 5.

Figure 8. Mobilised friction angle (assuming $c' = 0$) for hypothetical pore water pressure conditions defined by the pore pressure ratio ($r_u = r_u$) from $r_u = 0$ (dry slope condition) to $r_u = 0.426$ (water table at the ground surface for $\gamma = 23 \text{ kN m}^{-3}$).